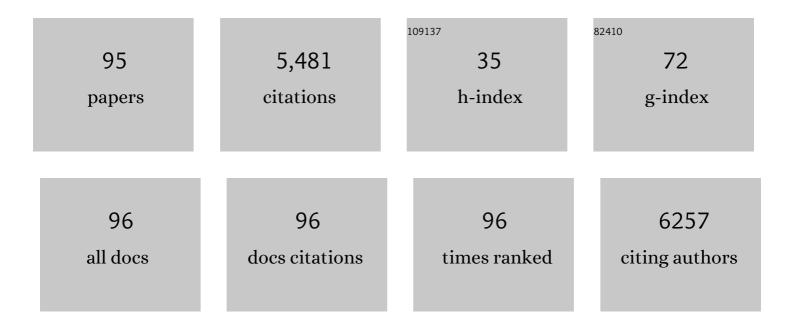
## **Deliang Chen**

List of Publications by Year in descending order

Source: https://exaly.com/author-pdf/3390046/publications.pdf Version: 2024-02-01



#	Article	IF	CITATIONS
1	Thermochromic VO2 for Energy-Efficient Smart Windows. Joule, 2018, 2, 1707-1746.	11.7	536
2	Nanoceramic VO2 thermochromic smart glass: A review on progress in solution processing. Nano Energy, 2012, 1, 221-246.	8.2	507
3	Microwave-assisted molten-salt rapid synthesis of isotype triazine-/heptazine based g-C3N4 heterojunctions with highly enhanced photocatalytic hydrogen evolution performance. Applied Catalysis B: Environmental, 2017, 203, 300-313.	10.8	312
4	Thermochromic VO <sub>2</sub> Thin Films: Solution-Based Processing, Improved Optical Properties, and Lowered Phase Transformation Temperature. Langmuir, 2010, 26, 10738-10744.	1.6	255
5	Nanoporous Thermochromic VO <sub>2</sub> Films with Low Optical Constants, Enhanced Luminous Transmittance and Thermochromic Properties. ACS Applied Materials & Interfaces, 2011, 3, 135-138.	4.0	247
6	VO2 thermochromic smart window for energy savings and generation. Scientific Reports, 2013, 3, 3029.	1.6	246
7	Size―and Shapeâ€Controlled Conversion of Tungstateâ€Based Inorganic–Organic Hybrid Belts to WO <sub>3</sub> Nanoplates with High Specific Surface Areas. Small, 2008, 4, 1813-1822.	5.2	183
8	Single-crystalline MoO3 nanoplates: topochemical synthesis and enhanced ethanol-sensing performance. Journal of Materials Chemistry, 2011, 21, 9332.	6.7	168
9	A Novel Solution Process for the Synthesis of VO <sub>2</sub> Thin Films with Excellent Thermochromic Properties. ACS Applied Materials & amp; Interfaces, 2009, 1, 2211-2218.	4.0	160
10	Solution-based fabrication of vanadium dioxide on F:SnO2 substrates with largely enhanced thermochromism and low-emissivity for energy-saving applications. Energy and Environmental Science, 2011, 4, 4290.	15.6	159
11	Effects of morphologies on acetone-sensing properties of tungsten trioxide nanocrystals. Sensors and Actuators B: Chemical, 2011, 153, 373-381.	4.0	141
12	The enhanced alcohol-sensing response of ultrathin WO <sub>3</sub> nanoplates. Nanotechnology, 2010, 21, 035501.	1.3	130
13	Sonochemical Synthesis of Ag/AgCl Nanocubes and Their Efficient Visibleâ€Lightâ€Driven Photocatalytic Performance. Chemistry - A European Journal, 2012, 18, 5192-5200.	1.7	128
14	Hierarchically plasmonic photocatalysts of Ag/AgCl nanocrystals coupled with single-crystalline WO3 nanoplates. Nanoscale, 2012, 4, 5431.	2.8	112
15	Microwave-assisted growth of In <sub>2</sub> O <sub>3</sub> nanoparticles on WO <sub>3</sub> nanoplates to improve H <sub>2</sub> S-sensing performance. Journal of Materials Chemistry A, 2014, 2, 18867-18874.	5.2	88
16	Normal-pressure microwave rapid synthesis of hierarchical SnO <sub>2</sub> @rGO nanostructures with superhigh surface areas as high-quality gas-sensing and electrochemical active materials. Nanoscale, 2014, 6, 13690-13700.	2.8	88
17	Oxygen vacancy engineered SrTiO <sub>3</sub> nanofibers for enhanced photocatalytic H <sub>2</sub> production. Journal of Materials Chemistry A, 2019, 7, 17974-17980.	5.2	88
18	Low-temperature and highly selective NO-sensing performance of WO3 nanoplates decorated with silver nanoparticles. Sensors and Actuators B: Chemical, 2013, 185, 445-455.	4.0	86

#	Article	IF	CITATIONS
19	WO3 quantum-dots electrochromism. Nano Energy, 2020, 68, 104350.	8.2	84
20	Effects of graphene on the microstructures of SnO2@rGO nanocomposites and their formaldehyde-sensing performance. Sensors and Actuators B: Chemical, 2018, 269, 223-237.	4.0	82
21	Graphene-Modified ZnO Nanostructures for Low-Temperature NO <sub>2</sub> Sensing. ACS Omega, 2019, 4, 4221-4232.	1.6	79
22	Hierarchical three-dimensional MoS2/GO hybrid nanostructures for triethylamine-sensing applications with high sensitivity and selectivity. Sensors and Actuators B: Chemical, 2020, 317, 128236.	4.0	67
23	Hierarchical Fe <sub>2</sub> O <sub>3</sub> @WO <sub>3</sub> nanostructures with ultrahigh specific surface areas: microwave-assisted synthesis and enhanced H <sub>2</sub> S-sensing performance. RSC Advances, 2015, 5, 328-337.	1.7	65
24	Effect of the Particle Size of Quartz Powder on the Synthesis and CO <sub>2</sub> Absorption Properties of Li <sub>4</sub> SiO <sub>4</sub> at High Temperature. Industrial & Engineering Chemistry Research, 2013, 52, 1886-1891.	1.8	64
25	Tungstate-Based Inorganicâ^'Organic Hybrid Nanobelts/Nanotubes with Lamellar Mesostructures: Synthesis, Characterization, and Formation Mechanism. Chemistry of Materials, 2007, 19, 1808-1815.	3.2	59
26	Utilization of coal gangue for the production of brick. Journal of Material Cycles and Waste Management, 2017, 19, 1270-1278.	1.6	58
27	Effects of a TiO <sub>2</sub> Buffer Layer on Solution-Deposited VO <sub>2</sub> Films: Enhanced Oxidization Durability. Journal of Physical Chemistry C, 2010, 114, 22214-22220.	1.5	55
28	Precursorâ€Engineering Coupled Microwave Moltenâ€Salt Strategy Enhances Photocatalytic Hydrogen Evolution Performance of g <sub>3</sub> N <sub>4</sub> Nanostructures. ChemSusChem, 2020, 13, 827-837.	3.6	54
29	Microwave-assisted preparation of hierarchical CuO@rGO nanostructures and their enhanced low-temperature H2S-sensing performance. Applied Surface Science, 2019, 476, 107-114.	3.1	53
30	Enhanced room-temperature ammonia-sensing properties of polyaniline-modified WO3 nanoplates derived via ultrasonic spray process. Sensors and Actuators B: Chemical, 2020, 312, 127892.	4.0	49
31	Enhancing thermochromic performance of VO2 films via increased microroughness by phase separation. Solar Energy Materials and Solar Cells, 2013, 110, 1-7.	3.0	43
32	Solvent-regulated solvothermal synthesis and morphology-dependent gas-sensing performance of low-dimensional tungsten oxide nanocrystals. Sensors and Actuators B: Chemical, 2014, 205, 391-400.	4.0	43
33	Mo <sub>2</sub> C-MXene/CdS Heterostructures as Visible-Light Photocatalysts with an Ultrahigh Hydrogen Production Rate. ACS Applied Energy Materials, 2021, 4, 12754-12766.	2.5	42
34	Synergetic integration of passivation layer and oxygen vacancy on hematite nanoarrays for boosted photoelectrochemical water oxidation. Applied Catalysis B: Environmental, 2021, 284, 119760.	10.8	40
35	Fabrication and Temperature-Dependent Field-Emission Properties of Bundlelike VO <sub>2</sub> Nanostructures. ACS Applied Materials & Interfaces, 2011, 3, 2057-2062.	4.0	37
36	High-Yield Preparation and Electrochemical Properties of Few-Layer MoS2 Nanosheets by Exfoliating Natural Molybdenite Powders Directly via a Coupled Ultrasonication-Milling Process. Nanoscale Research Letters, 2016, 11, 409.	3.1	32

#	Article	IF	CITATIONS
37	Ultrabroadband red luminescence of Mn <sup>4+</sup> in MgAl <sub>2</sub> O <sub>4</sub> peaking at 651 nm. Dalton Transactions, 2020, 49, 5711-5721.	1.6	31
38	Microwave-assisted synthesis of hierarchically porous Co3O4/rGO nanocomposite for low-temperature acetone detection. Journal of Colloid and Interface Science, 2021, 594, 690-701.	5.0	31
39	Investigation on g-C3N4/rGO/TiO2 nanocomposite with enhanced photocatalytic degradation performance. Journal of Physics and Chemistry of Solids, 2021, 156, 110181.	1.9	30
40	Effects of the Particle Size of BaTiO3 Fillers on Fabrication and Dielectric Properties of BaTiO3/Polymer/Al Films for Capacitor Energy-Storage Application. Materials, 2019, 12, 439.	1.3	28
41	Construction and enhanced low-temperature H2S-sensing performance of novel hierarchical CuO@WO3 nanocomposites. Journal of Alloys and Compounds, 2019, 785, 367-373.	2.8	28
42	Simple Synthesis and Characterization of Hexagonal and Ordered Al–MCM–41 from Natural Perlite. Minerals (Basel, Switzerland), 2019, 9, 264.	0.8	27
43	Comparative insight into effect of hybridizing potassium and hydrogen ions on photocatalytic Reduction/Oxidization behavior of g-C3N4 nanocrystals. Chemical Engineering Journal, 2021, 417, 129187.	6.6	27
44	Steering charge kinetics in W2C@C/TiO2 heterojunction architecture: Efficient solar-light-driven hydrogen generation. Applied Catalysis B: Environmental, 2019, 255, 117760.	10.8	25
45	Enhanced triethylamine-sensing properties of hierarchical molybdenum trioxide nanostructures derived by oxidizing molybdenum disulfide nanosheets. Journal of Colloid and Interface Science, 2022, 605, 624-636.	5.0	25
46	Preparation and characterization of ZrB2-SiC ultra-high temperature ceramics by microwave sintering. Frontiers of Materials Science in China, 2010, 4, 276-280.	0.5	24
47	Lithium Difluorophosphate as an Effective Additive for Improving the Initial Coulombic Efficiency of a Silicon Anode. ChemElectroChem, 2020, 7, 3743-3751.	1.7	24
48	A simple and recyclable molten-salt route to prepare superthin biocarbon sheets based on the high water-absorbent agaric for efficient lithium storage. Carbon, 2020, 157, 286-294.	5.4	23
49	In situ formation of Au/SnO 2 nanocrystals on WO 3 nanoplates as excellent gas-sensing materials for H 2 S detection. Materials Chemistry and Physics, 2014, 148, 1099-1107.	2.0	22
50	Factors influencing formation of highly dispersed BaTiO3 nanospheres with uniform sizes in static hydrothermal synthesis. Journal of Nanoparticle Research, 2015, 17, 1.	0.8	22
51	Promote the electrocatalysis activity of amorphous FeOOH to oxygen evolution reaction by coupling with ZnO nanorod array. Journal of Solid State Electrochemistry, 2020, 24, 905-914.	1.2	22
52	Coupled ultrasonication-milling synthesis of hierarchically porous carbon for high-performance supercapacitor. Journal of Colloid and Interface Science, 2018, 528, 208-224.	5.0	21
53	Intense deep-red zero phonon line emission of Mn <sup>4+</sup> in double perovskite La <sub>4</sub> Ti <sub>3</sub> O <sub>12</sub> . Physical Chemistry Chemical Physics, 2019, 21, 25108-25117.	1.3	21
54	Enhanced selective response to nitric oxide (NO) of Au-modified tungsten trioxide nanoplates. Materials Chemistry and Physics, 2013, 143, 461-469.	2.0	20

#	Article	IF	CITATIONS
55	2D/1D V2O5 Nanoplates Anchored Carbon Nanofibers as Efficient Separator Interlayer for Highly Stable Lithium–Sulfur Battery. Nanomaterials, 2020, 10, 705.	1.9	20
56	Microwave-assisted reconstruction of spent graphite and its enhanced energy-storage performance as LIB anodes. Surfaces and Interfaces, 2021, 24, 101098.	1.5	20
57	Polypropylene/combinational inorganic filler microâ€/nanocomposites: Synergistic effects of microâ€/nanoscale combinational inorganic fillers on their mechanical properties. Journal of Applied Polymer Science, 2010, 115, 624-634.	1.3	19
58	The influence of additive and temperature on thermal shock resistance of ZrB2 based composites fabricated by Spark Plasma Sintering. Materials Chemistry and Physics, 2020, 240, 122061.	2.0	19
59	Microsized Red Luminescent MgAl <sub>2</sub> O <sub>4</sub> :Mn <sup>4+</sup> Single-Crystal Phosphor Grown in Molten Salt for White LEDs. Inorganic Chemistry, 2020, 59, 18374-18383.	1.9	19
60	A comparative study on reactions of n-alkylamines with tungstic acids with various W–O octahedral layers: Novel evidence for the "dissolution–reorganization―mechanism. Materials Chemistry and Physics, 2011, 125, 838-845.	2.0	17
61	Preparation of Magnetic Kaolinite Nanotubes for the Removal of Methylene Blue from Aqueous Solution. Journal of Inorganic and Organometallic Polymers and Materials, 2018, 28, 790-799.	1.9	17
62	High temperature induced S vacancies in natural molybdenite for robust electrocatalytic nitrogen reduction. Journal of Colloid and Interface Science, 2021, 599, 849-856.	5.0	16
63	Synthesis and growth mechanism of ZnO rodâ€ŀike nanostructures by a microwaveâ€assisted Iowâ€ŧemperature aqueous solution route. Crystal Research and Technology, 2014, 49, 298-302.	0.6	14
64	ZrB <sub>2</sub> ‣iC <sub>w</sub> ceramic composites synthesized by in situ reaction and spark plasma sintering. International Journal of Applied Ceramic Technology, 2017, 14, 845-850.	1.1	13
65	Lauric Acid Hybridizing Fly Ash Composite for Thermal Energy Storage. Minerals (Basel, Switzerland), 2018, 8, 161.	0.8	13
66	Bio-inspired SiO2-hard-template reconstructed g-C3N4 nanosheets for enhanced photocatalytic hydrogen evolution. Catalysis Science and Technology, 2020, 10, 4655-4662.	2.1	13
67	TiO2-Seeded Hydrothermal Growth of Spherical BaTiO3 Nanocrystals for Capacitor Energy-Storage Application. Crystals, 2020, 10, 202.	1.0	13
68	Which is Better for Nanomedicines: Nanocatalysts or Singleâ€Atom Catalysts?. Advanced Healthcare Materials, 2021, 10, e2001897.	3.9	13
69	Novel Synthesis of Hierarchical Tungsten Carbide Microâ€∕Nanocrystals from a Singleâ€&ource Precursor. Journal of the American Ceramic Society, 2010, 93, 3997-4000.	1.9	11
70	Linear-Polyethyleneimine-Templated Synthesis of N-Doped Carbon Nanonet Flakes for High-performance Supercapacitor Electrodes. Nanomaterials, 2019, 9, 1225.	1.9	11
71	Solution growth of millimeterâ€scale Na <sub>2</sub> SiF <sub>6</sub> single crystals for Mn <sup>4+</sup> â€doping as red phosphor. Journal of the American Ceramic Society, 2021, 104, 5077-5085.	1.9	11
72	Linear-PEI-Derived Hierarchical Porous Carbon Nanonet Flakes Decorated with MoS <sub>2</sub> as Efficient Polysulfides Stabilization Interlayers for Lithium–Sulfur Battery. Energy & Fuels, 2021, 35, 10303-10314.	2.5	11

#	Article	IF	CITATIONS
73	Synthesis and Characterization of Ti <scp>N</scp> â€coated Cubic Boron Nitride Powders. International Journal of Applied Ceramic Technology, 2014, 11, 946-953.	1.1	10
74	Single-source precursor synthesis of nitrogen-doped porous carbon for high-performance electrocatalytic ORR application. Ceramics International, 2019, 45, 8354-8361.	2.3	10
75	Temperature-dependent elastic stiffness constants of fcc-based metal nitrides from first-principles calculations. Journal of Materials Science, 2014, 49, 424-432.	1.7	9
76	Synthesis and characterization of carbonâ€doped ZnSn(OH) <sub>6</sub> with enhanced photoactivity by hydrothermal method. Crystal Research and Technology, 2016, 51, 11-15.	0.6	8
77	BaTiF <sub>6</sub> :Mn <sup>4+</sup> Red Phosphor: Synthesis of Single Crystals at Room Temperature and the High Hydrolysis-Resistant Property. Inorganic Chemistry, 2021, 60, 13212-13221.	1.9	7
78	Removal of persistent acetophenone from industrial waste-water via bismuth ferrite nanostructures. Chemosphere, 2022, 302, 134750.	4.2	7
79	Properties of Glassâ€Ceramics Synthesized from Blast Furnace Slag with Different Sizes. Steel Research International, 2011, 82, 741-745.	1.0	6
80	Synthesis of ZnSn(OH) <sub>6</sub> regular octahedrons by a simple hydrothermal process. Crystal Research and Technology, 2011, 46, 1079-1085.	0.6	6
81	Preparation of hierarchical NiCo2O4 self-assembled by lamellar flakes and its microwave absorption. Journal of Materials Science: Materials in Electronics, 2019, 30, 17358-17362.	1.1	6
82	Composite K <sub>2</sub> Mo <sub>4</sub> O <sub>13</sub> /α-MoO <sub>3</sub> nanorods: sonochemical preparation and applications for advanced Li <sup>+</sup> /Na <sup>+</sup> pseudocapacitance. Journal of Materials Chemistry A, 2019, 7, 10954-10961.	5.2	6
83	Hydrothermal synthesis and characterization of micro/nanostructured ZnSn(OH) <sub>6</sub> /ZnO composite architectures. Crystal Research and Technology, 2011, 46, 1175-1180.	0.6	5
84	Large Scale Synthesis of Nanopyramidal-Like VO2 Films by an Oxygen-Assisted Etching Growth Method with Significantly Enhanced Field Emission Properties. Nanomaterials, 2019, 9, 549.	1.9	5
85	Effect of Co-Doping on Thermoelectric Properties of n-Type Bi2Te3 Nanostructures Fabricated Using a Low-Temperature Sol-Gel Method. Nanomaterials, 2021, 11, 2719.	1.9	5
86	Superior electrocatalytic ORR performance of Melaleuca Leucadendron L barks derived hierarchical porous carbon with abundant atom-scale vacancies and multiheteroatoms. Ceramics International, 2022, 48, 11111-11123.	2.3	5
87	Morphology control of anisotropic BaTiO3 and BaTiOF4 using organic–inorganic interaction. Journal of Crystal Growth, 2009, 311, 589-592.	0.7	4
88	Controlled synthesis of ZnO nanostructures with different morphologies in microemulsions. Crystal Research and Technology, 2012, 47, 754-762.	0.6	4
89	Valence State Control of Manganese in MgAl <sub>2</sub> O <sub>4</sub> :Mn <sup>4+</sup> Phosphor by Varying the Al <sub>2</sub> O <sub>3</sub> Crystal Form. Wuji Cailiao Xuebao/Journal of Inorganic Materials, 2021, 36, 513.	0.6	4
90	Advances in Valence State Analysis of Manganese in Mn <sup>4+</sup> -activated Red Phosphors for White LEDs. Chinese Journal of Luminescence, 2020, 41, 1195-1213.	0.2	4

#	Article	IF	CITATIONS
91	Co-Ni Basic Carbonate Nanowire/Carbon Nanotube Network With High Electrochemical Capacitive Performance via Electrochemical Conversion. Frontiers in Chemistry, 2021, 9, 655025.	1.8	3
92	Porous Tungsten Carbide Nanoplates Derived from Tungsten Trioxide Nanoplates. Journal of the American Ceramic Society, 2012, 95, 3370-3373.	1.9	2
93	Nucleation of epitaxial graphene on SiC substrate by thermal annealing and chemical vapor deposition. Applied Physics A: Materials Science and Processing, 2013, 112, 349-355.	1.1	2
94	Porous three-dimensional core-shell WC@C nanocomposite derived from tungsten-containing inorganic-organic hybrid precursor. Materials Letters, 2016, 185, 331-334.	1.3	1
95	Thermal Performance and Interfacial Aspects of Kaoliniteâ€Based Stearic Acid Composite in the Presence of Nitric Acid. ChemistrySelect, 2019, 4, 13109-13114.	0.7	0